DRAFT 12/26/2022

Title: Sensitivity to direction and velocity of fast frequency chirps in the inferior colliculus

Paul W. Mitchell, Kenneth S. Henry, and Laurel H. Carney

Departments of Biomedical Engineering, Neuroscience, and Otolaryngology, University of Rochester

Abstract

Neurons in the mammalian inferior colliculus (IC) are selective for the direction of fast frequency sweeps (chirps) contained in Schroeder-phase harmonic complexes (SCHR). This selectivity points to a feature sensitivity to fast-chirp direction and velocity in the IC potentially shared by all mammals. Here, we introduced a novel stimulus consisting of Aperiodic Random Chirps (ARC) to distinguish neurons' sensitivity to chirp direction and velocity from the confounding periodicity of SCHR stimuli. Extracellular, single-unit recordings were made in the IC of Dutch-belted rabbits. SCHR stimuli had a range of velocities and periodicities. ARC stimuli with matched velocities and sinusoidally amplitude-modulated (SAM) noise were also presented. The prevalence of direction sensitivity and direction bias to chirps in SCHR and ARC responses was quantified, revealing that the majority of IC neurons (90.5%) were selective to SCHR-chirp direction and that sensitivity to the direction of aperiodic chirps was nearly universal (99.6%). Rate-velocity functions were constructed from ARC responses, revealing that neurons were often sensitive to the direction of the lowest-velocity chirps used and were insensitive to the direction of the highest-velocity chirps used. ARC and SAM noise responses were combined using a generalized linear model (GLM) to predict SCHR response rates. The GLM analysis revealed that both velocity and periodicity cues were required to explain SCHR responses. In general, velocity cues have a stronger effect on responses for stimuli with lower F0s. This result has implications for neural encoding of complex sounds that combine envelope periodicities and frequency-sweeps.

Introduction

The inferior colliculus (IC) receives convergent excitatory and inhibitory inputs from several auditory brainstem nuclei, resulting in a variety of complex response properties, such as different types of frequency tuning (reviewed in Davis, 2005) and sensitivity to interaural differences, duration, and amplitude modulation (AM) (Casseday et al., 1994; Kock and Grothe,1998; Caspary et al., 2002; Pollak et al., 2001; Yin et al., 2019). Sensitivity of IC neurons to frequency-modulated (FM) sweep direction and velocity has also been extensively studied. Starting with Suga (1965), studies of bat IC responses have reported neurons that prefer, or even respond exclusively, to a selected FM direction, a possible adaptation for echolocation (Suga, 1965; Fuzesery, 1994; Fuzessery and Hall, 1996; Gordon and O'Neill, 1998; Pollak et al., 2011). Additionally, sounds with time and frequency modulations having statistics comparable to those of spectral-peak, or formant-frequency, transitions in real-world sounds, such as animal vocalizations or speech, have been used to characterize IC spectrotemporal receptive fields (STRFs) (Escabi and Schreiner, 2002; Escabi et al., 2003; Andoni et al., 2007; Wooley et al., 2009).

Recently, IC FM sensitivity to the direction and velocity of FM sweeps has been discovered in gerbils (Steenken et al., 2022). This study used Schroeder-phase (SCHR) harmonic complexes, a useful stimulus for studying FM. The harmonic components of SCHR stimuli have flat magnitude spectra and curved phase spectra that create stimuli with maximally flat envelopes (Schroeder, 1970). The phase differences across harmonic components result in linear frequency sweeps within each fundamental period, extending from the fundamental frequency (F0) to the highest harmonic component. SCHR sensitivity is notable for the sheer speed of the FM, with sweeps traveling from F0 to the maximum harmonic (here, 16 kHz) over the fundamental period (here, between 2.5 and 20 ms). The resulting velocities are faster than commonly considered FM signals such as formant transitions (Liberman and Mattingly, 1989).

We refer to these fast SCHR sweeps as SCHR chirps. In this paper we report sensitivity in rabbit IC to the direction and velocity of SCHR chirps. Rabbits do not produce vocalizations containing fast FM, and therefore presumably lack special adaptations for processing fast FM (Awan et al., 2014). Instead, rabbits have representative mammalian hearing, with average high-frequency hearing among similarly-sized mammals, and low-frequency hearing similar to humans (Masterson and Heffner, 1980).

IC sensitivity to SCHR chirps suggests a novel feature sensitivity in the mammalian auditory system (Steenken et al., 2022). However, this sensitivity is not yet fully understood. IC neurons are tuned for periodicity (Schreiner and Langer, 1988; Krishna and Semple, 2000; Nelson and Carney, 2007; Kim et al., 2020), therefore the periodicity of SCHR stimuli may confound estimates of neural sensitivity to chirps. Using the Aperiodic Random Chirp (ARC) stimulus, we analyzed responses to aperiodic SCHR chirps, allowing the quantification of velocity sensitivity in stimuli without periodicity. Sensitivity to the direction of FM chirps was present in nearly all IC neurons. We used the generalized linear model (GLM) to predict SCHR chirp responses based on responses to ARC stimuli and SAM noise. For most neurons, including both periodicity and velocity terms increased the variance explained by the model.

Methods

Extracellular, single-unit recordings were made in the central nucleus of the IC (ICC) of six female Dutch-belted rabbits (*Oryctolagus cuniculus*). Rabbits were obtained from Envigo (Denver, PA). The age of the animals during experiments ranged from 1-5 years, during which DPOAEs and IC neural thresholds were used to confirm normal hearing (Whitehead et al., 1992). Animals were euthanized when their DPOAE magnitudes decreased or neural thresholds increased. All methods were approved by the University of Rochester Committee on Animal Resources.

Recordings

Recordings were made in daily two-hour sessions in sound-attenuated booths (Acoustic Systems, Austin, TX, USA). To prevent head movement of the awake rabbits, a headbar (metal or 3D-printed plastic) was surgically affixed to the skull using stainless-steel screws and dental acrylic. Rabbits were anesthetized using ketamine (66 mg/kg) and xylazine (2 mg/kg), administered intramuscularly, for headbar placement, craniotomy, and electrode placements (below). Rabbits were wrapped in a towel and secured in a custom-made chair to limit movement during recording sessions.

Recordings were made using four tetrodes, consisting of four 18-μm platinum-iridium epoxy-coated wires (California Fine Wire Co., Grover Beach, CA, USA), plated with platinum black to obtain impedances of approximately 0.1 – 2 MOhms. Tetrodes were surgically implanted in the ICC via a small (~2mm diameter) craniotomy in the top of the skull. Stainless-steel guidetubes protected the tetrodes, which were positioned just dorsal to the ICC and then advanced through the ICC using a manual microdrive (Five-drive, Neuralynx, Inc., Bozeman, MT, USA). Tetrodes were advanced before or after recording sessions. The microdrive and tetrodes were surgically replaced every few months as needed to vary the recording location. Neural recordings were made using an RHD recording system (Intan Technologies, LLC., Los Angeles, CA, USA), with Intan software running on a Windows PC.

Stimuli were generated using custom MATLAB (Mathworks, Natick, MA, USA) code, a MOTU audio interface (16A, Mark of the Unicorn, Cambridge, MA, USA), and a Benchmark digital-to-analog converter (DAC3 HGC, Benchmark Media Systems, Inc., Syracuse, NY, USA). Etymotic ER2 earphones (Etymotic Research, Inc., Elk Grove Village, IL, USA) were used to present sound stimuli via custom ear molds (Hal-Hen Company, Inc., Garden City Park, New York, USA). Prior to every session, stimuli were calibrated using ER-7C or ER-10B+ probe-tube microphones (Etymotic Research, Inc., USA) and an Etymotic probe tube. The calibration curve

(magnitude and phase) was included in a pre-emphasis filter that compensated all stimuli for the acoustic system's frequency response.

Action potential times and waveforms were extracted from neural recordings using custom MATLAB applications. To identify single-unit events, the voltage recording was filtered using a 4th-order Butterworth bandpass filter (300 – 3000 Hz). An action potential was identified when the filtered voltage signal exceeded a threshold, defined as four standard deviations of the voltage signal. Action potentials were sorted into clusters, presumed to represent different neurons, using features of the waveforms, primarily the slope of the waveform repolarization (Schwarz et al., 2012). Single-units were identified when less than 2% of the interspike intervals were smaller than 1 ms. Neurons studied in consecutive sessions were considered to be unique only when both tetrode the location and response properties changed.

Stimuli

Recording sessions began by presenting wideband (100 Hz – 15 kHz) noise to the two ears to characterize the binaural responses. Noise stimuli were presented to the contralateral ear, ipsilateral ear, and both ears at 3, 13, and 33 dB SPL spectrum level, with 1-s durations and 3 repetitions each. Then, a set of stimuli was presented to define basic response properties, including frequency response maps, modulation transfer functions, and rate-velocity functions.

To generate frequency response maps, a randomly-ordered sequence of 0.2-s-duration tones at frequencies ranging from 250 Hz – 16 kHz was presented at 13, 33, 53, and 73 dB SPL. Tones were presented either contralaterally or diotically and were separated by 0.4 s of silence. Each stimulus condition was presented three times. Response maps, plots of average discharge rate vs. frequency at each stimulus level, were used to estimate characteristic frequency (CF), the frequency for which threshold was lowest.

Modulation transfer functions (MTF) were estimated by computing the average rate in response to 100% sinusoidal amplitude-modulated (AM) noise as a function of modulation frequency, over a range of 2 – 350 Hz. The wideband noise (100 Hz – 10 kHz) was 1 s in duration, including 50-ms raised-cosine on/off ramps, separated by 0.5 s of silence, presented diotically. Modulation frequencies were presented in random order, with 5 repetitions of each. Stimuli were presented at a spectrum level of 33 dB (overall level of 73 dB SPL). MTF categorization was based on criteria that were slightly modified from Kim et al. (2020), MTF types were categorized as band-enhanced (BE) if (1) the MTF had three consecutive points greater than the product of the unmodulated rate (r_{um}) and a criterion K, and (2) the MTF did not have more than one point below the product of r_{um} and $1/K$. Similarly, MTFs were categorized as band-suppressed (BS) if (1) the MTF had three consecutive points less than r_{um}/K, and (2) the MTF did not have more than one point above $r_{um}K$. For this study, K was set to 1.2, i.e., a 20% increase in rate with respect to the unmodulated response was required for BE MTFs and a 20% decrease was required for BS MTFs. MTFs that had both enhanced and suppressed bands that met the above criteria were categorized as hybrid MTFs. In the population of neurons studied, 43.3% were BS, 17.0% were BE, 24.5% were hybrid, and 15.2% had flat or unusual MTF shapes. For BE neurons, the peak of the MTF was designated the best modulation frequency (BMF). For BS neurons, the lowest point in the MTF was designated the trough modulation frequency (TMF), and for hybrid neurons both a BMF and TMF were identified.

SCHR stimuli were produced using the phase spectrum introduced in Schroeder (1970) (Fig. 1A-D). For a harmonic complex with n components, the phase of the nth component was described by $\theta_n = C\pi n(n+1)/N$, where N is the total number of harmonic components, and C is a scalar that describes the phase-direction and duty cycle of the stimulus. A random sequence of SCHR stimuli were presented, with F0 equal to 50, 100, 200, or 400 Hz and C

equal to -1, -0.5, 0, 0.5, or 1. For all cases, the frequency of the highest harmonic component was 16 kHz. The number of harmonic components, N, depended on F0, and ranged between 40 and 320. Thirty repetitions of each F0 and C combination were presented. Stimuli were presented diotically at 63 dB SPL, with a duration of 0.4 seconds followed by 0.6 seconds of silence, with 25-ms raised cosine on/off ramps. Average discharge rates over the stimulus duration were calculated for each F0 and C combination. Receiver-operating-characteristic (ROC) analysis was used to evaluate neural direction selectivity between SCHR conditions with equivalent F0 and C-values of opposite signs (i.e. F0 = 50 Hz, C = ±1) (Egan, 1975). Neurons were deemed significantly biased if the area under the ROC curve (AUC) was above 70.7% or below 29.3%. Additionally, the direction of the bias was designated negative for neurons with AUCs above 70.7% (indicating greater mean response rate for the negative Schroeder stimulus) and positive for neurons with AUCs below 29.3%. The ROC threshold of 70.7% (and 29.3%) was chosen because it is equivalent to the targeted level on the psychometric function by a two-down, one-up psychophysical procedure (Levitt, 1971).

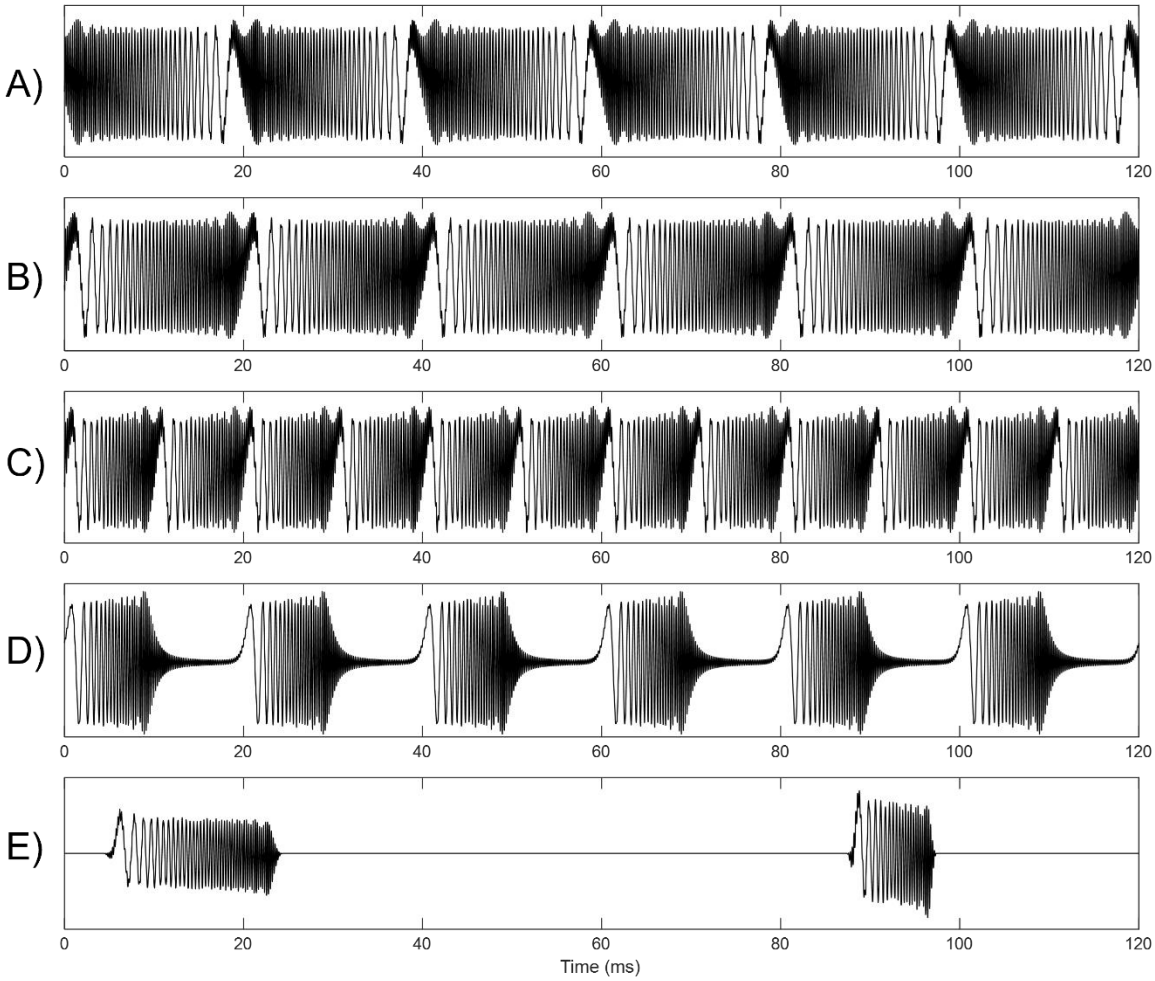

Figure 1 – Stimulus waveforms of SCHR and ARC stimuli. Note that the maximum harmonic in this figure is 5 kHz for clarity; in the actual stimuli, maximum harmonic was 16 kHz. (A) SCHR with F0 = 50 Hz, C = 1. (B) SCHR with F0 = 50 Hz, C = -1. (C) SCHR with F0 = 100 Hz, C = -1. (D) SCHR with F0 = 50 Hz, C = -0.5. (E) Two consecutive ARC-stimulus chirps separated by silence.

Rate-velocity functions (RVFs) were based on responses to ARC (aperiodic random chirp) stimuli. ARC stimuli were isolated SCHR chirps, or single fundamental periods extracted from a SCHR stimulus, equivalent to one full SCHR chirp spanning F0 to the maximum harmonic, or vice versa (Fig. 1E). To produce the stimulus waveforms, first, a random sequence of chirp velocities was generated, which were equivalent to SCHR F0s of 25, 50, 100, 200, 400, and 600 Hz. Chirp direction (upward or downward) was also randomly varied across stimuli.

These parameters together resulted in ARCs with velocities ±0.23, ±0.42, ±0.73, ±1.26, ±2.13, and ±2.84 octaves/ms. Each combination of velocity and direction was presented a total of 42 times within each full stimulus, in random order. ARCs were randomly spaced, using 40 – 60 ms uniformly distributed inter-chirp intervals, to avoid periodicity. The full stimulus set was presented 20 times. Each individual chirp had raised-cosine on/off ramps applied, with duration equivalent to 10% of chirp duration. Finally, the level of individual chirps was scaled by $-10 \times \log_{10}(T/T_{ref})$, where T is the duration of the chirp and T_{ref} = 2.5 ms (the duration equivalent to a SCHR chirp with F0 = 400 Hz). This scaling ensured that energy was equivalent across chirps of different durations. Stimuli were presented diotically at 68 dB SPL. Extracting response rates from ARC-stimulus responses was complicated by variation in onset response latency and the presence of offset responses in many neurons. The response-rate calculation began by locating the peak rate in the peristimulus time histogram (PSTH) over a time window starting at chirp onset with a duration matched to that of the chirp plus the minimum spacing between chirps (i.e., chirp duration + 40 ms) (Fig. 2). Then, response rate was calculated by summing spikes over a 20-ms time window centered at the peak of the PSTH, except where this window would cross the minimum (0 ms) or maximum (chirp duration + 40 ms) of the PSTH time axis. ROC analysis of ARC rates was performed in an identical manner as for SCHR rates. ARC rates were used to generate RVFs, which described how a neuron's rate changed as a function of chirp velocity (Figs. 3-7). The RVF describes a neuron's response profile to aperiodic chirps of different velocities, allowing salient response properties to be easily identified.

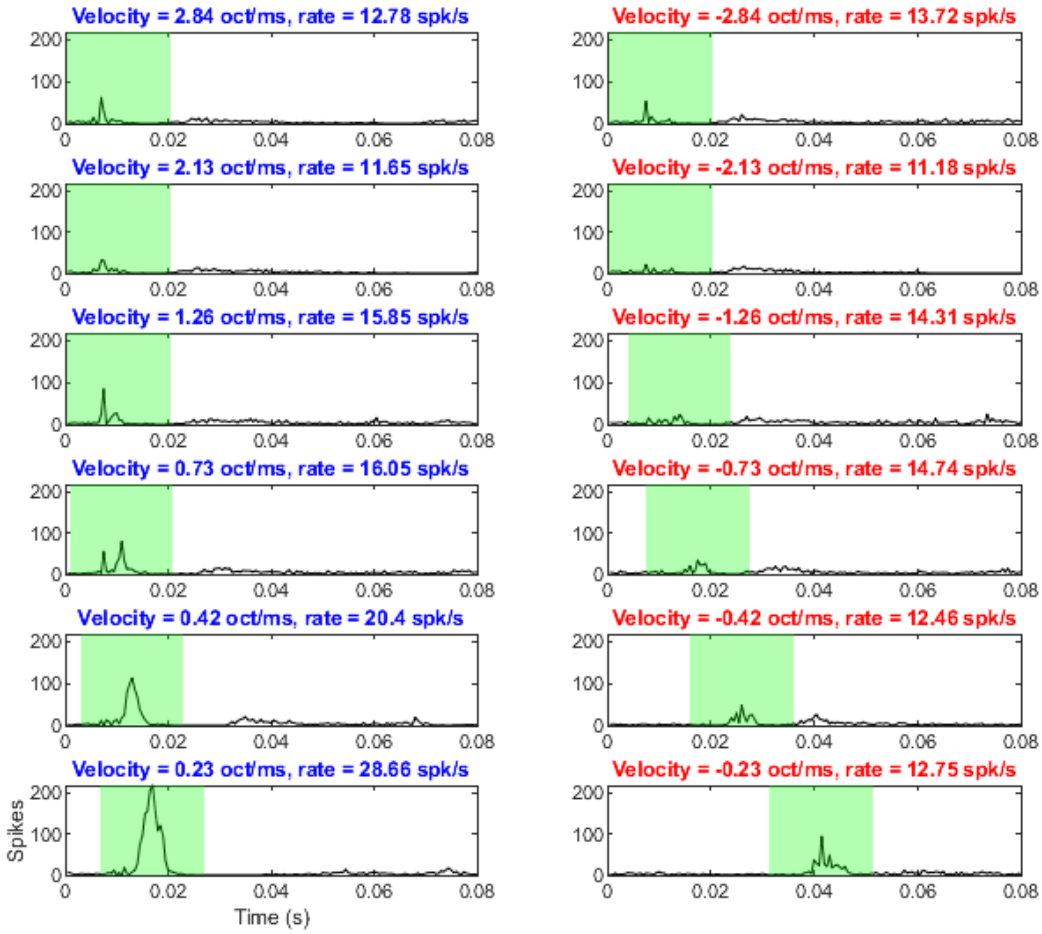

Figure 2 – A visual depiction of ARC-stimulus rate calculation. Black lines illustrate PSTHs (bin size = 0.5 ms) of responses to ARCs of different velocities. The left column (blue titles) contains positively-sloped ARCs (equivalent direction to -SCHR chirps), and the right column (red titles) contains negatively-sloped ARCs (equivalent direction to +SCHR chirps). The green rectangles indicate the placement of the 20-ms window over which response rate is calculated. Generally, the window is centered at the peak of the PSTH, except where that would cause the window to cross the minimum (0 ms) or maximum (80 ms) time intervals (e.g. Velocity = 2.84 oct/ms PSTH, top left).

Analysis

Principal Component Analysis (PCA) was performed on the RVFs using the MATLAB function PCA (2021b, MathWorks) on the set of RVFs (247 in total). RVFs were normalized by their individual peak rates before PCA analysis.

SCHR responses were predicted based on MTFNs and RVFs using the generalized linear model (GLM). First, SCHR rates, MTFNs, and RVFs were normalized by each of their maximum rates. For the responses to periodic stimuli, (MTFN and SCHR), cycle rate was used, defined as the average rate per fundamental period (T0). Cycle rate (spikes/cycle) was used to counteract the strong phase-locking of many neurons to the fundamental frequency, which resulted in average rates that disproportionally increased with F0 using the conventional calculation (spikes/second). For the aperiodic stimulus (ARC), rate was calculated using the previously mentioned method of summing spikes over a window up to 40-ms in duration centered around the peak of the PSTH. Following this, MTFNs and RVFs were projected onto the SCHR space such that each of the 16 SCHR rates was associated with one point on the MTFN and one point on the RVF. The SCHR rates can be visualized as a surface on this periodicity/velocity grid (Fig. 14, upper left). The periodicity and velocity of each SCHR point on this grid was matched with the closest available modulation frequency and velocity from the MTFN and RVF, respectively (data were not interpolated), creating a feature vector for the neurons' pure response to periodicity and velocity changes. Then, a relationship between the periodicity and velocity feature vectors and SCHR rates was defined for the GLM as follows:

$$R_S = b_P R_P + b_V R_V + b_I (R_P * R_V) + b_0 \quad , \qquad \text{(Eqn. 1)}$$

where R_P and R_V refer to rates of the periodicity and velocity feature vectors, respectively. R_S is the predicted response to SCHR stimuli in cycle rate, and b_n are the GLM coefficients. There were three terms in the GLM—a periodicity term, a velocity term, and an interaction term. GLM

coefficients were estimated using the MATLAB function glmfit (2021b, MathWorks), with the distribution argument set to normal and constant argument set to on. The GLM coefficients were b_P, the periodicity coefficient, b_V, the velocity coefficient, b_I, the interaction term coefficient, and b_0, a constant. After the SCHR rate prediction was calculated using estimated coefficients, the coefficient of determination (R^2) of the predicted and recorded SCHR cycle rates was determined to assess prediction quality. This process was repeated for two additional, simpler GLMs:

$$R_S = b_1 R_P + b_0 \quad , \quad \text{and} \qquad \text{(Eqn. 2)}$$

$$R_S = b_1 R_V + b_0 \quad . \qquad \text{(Eqn. 3)}$$

These simpler GLMs depended only on one feature vector and thus could be used to assess the importance of periodicity or velocity alone. The coefficient of determination (R^2) of these two model predictions were obtained and used to measure the impact of the two features on neurons' SCHR responses.

The following equation was used to calculate the contribution of velocity-cues to the total explainable variance:

$$Percent\ contribution\ of\ velocity\ to\ R^2 = \frac{\left(R^2{}_{combined} - R^2{}_{periodicity}\right)}{R^2{}_{combined}} \times 100 \ , \qquad \text{(Eqn. 4)}$$

where $R^2{}_{combined}$ and $R^2{}_{periodicity}$ refer to the coefficient of determination of the combined model (Eqn. 1) and periodicity-alone model (Eqn. 2), respectively. Equation 4 allowed the amount of additional variance explained by the inclusion of velocity (either in the velocity term or interaction term in Eqn. 1) to be directly quantified.

Code and data will be made available on OSF.

Results

A. Sensitivity of IC neurons to direction and velocity of SCHR chirps was diverse

Data were recorded over a span of 330 sessions and included recordings from 335 unique single units. Response properties of single-unit neurons are illustrated using RMs, MTFs, RVFs, and dot rasters of SCHR responses (Figs. 3-7). The neural sensitivity to chirps was first noted in SCHR dot rasters, which illustrate salient trends in the responses of each neuron, such as detailed timing and rate differences between SCHR conditions that differ in direction or velocity. RMs were used to determine CF; these plots also reveal off-CF inhibitory regions. MTFs were categorized as BE, BS, or hybrid, and were used to identify BMF and/or TMF. Lastly, RVFs were constructed from ARC-stimuli responses, which differ from SCHR responses because they reflect the neural sensitivity to velocities of single chirps removed from a periodic context. Altogether, RMs, MTFs, and RVFs provided a response profile from which underlying mechanisms of SCHR-chirp sensitivity were hypothesized—specifically, that SCHR responses were the result of a combination of modulation tuning, off-CF inhibition in the RM, and chirp velocity tuning, with the relative importance of these influences differing between neurons. Figures 3-7 provide several diverse examples that demonstrate how the SCHR response profile of a given neuron may be influenced by a combination of modulation tuning, chirp velocity tuning, and off-CF inhibition.

Figure 3 shows an example of a unit with a complex SCHR response that was not fully explainable by the responses to characterizing stimuli. The SCHR raster (Fig. 3C) displays stronger rates in response to positive-chirps (red dots) at the lowest chirp velocity, 50 Hz, C = ±1. This positive-chirp preference was not maintained for higher velocities. The neuron's MTF (Fig. 3B) was BS, with a trough spanning modulation frequencies that included the SCHR F0s of

50 and 100 Hz, and with relatively less suppression at modulation frequencies matching the F0s of 200 and 400 Hz. If the MTF solely predicted this neuron's SCHR response, responses to 50- and 100-Hz SCHR chirps would have be nearly entirely suppressed. However, the neuron's response was robust for all 50-Hz chirp conditions except for 50 Hz, C = -1, suggesting that the direction and/or velocity sensitivity to these chirps overcame the suppression observed in the MTF. Thus, the MTF alone could not simply explain this neuron's SCHR response profile. Meanwhile, the RM (Fig. 3A) was sharply tuned to 1.2 kHz with a low threshold (13 dB SPL), and revealed a high-frequency inhibitory region at high sound levels. If the neuron's SCHR response were dependent on this asymmetrical sideband inhibition, it would have responded more strongly to upward chirps (i.e. –SCHR) than to downward chirps (Gordon and O'Neill, 1998). However, the neuron instead responded more strongly to +SCHR (downward) chirps than –SCHR (upward) for 50 Hz F0. Therefore, the neuron's asymmetrical sideband inhibition alone could not explain the SCHR response. The neuron's RVF (Fig. 3D) shows an increased response to upward-sweeping chirps (-SCHR, blue) compared to downward-sweeping chirps (+SCHR, red) for most velocity-pairs, with the exception of ±0.23 oct/ms (equivalent to SCHR with F0 25 Hz, C = ±1), at which rates were slightly higher for the downward-sweeping chirp. For the most part, the RVF did not adequately reflect SCHR responses either; SCHR rates did not consistently favor upward chirps (-SCHR). Instead, direction selectivity was only strong at 50 Hz, C = ±1, showing a selectivity for downward SCHR chirps (+SCHR), while the RVF showed a selectivity for upward chirps for the equivalent velocity pair (±0.42 oct/ms). That the RM, MTF, nor RVF simply predict the SCHR response suggests that the SCHR response may have been driven by an interaction between the three feature sensitivities.

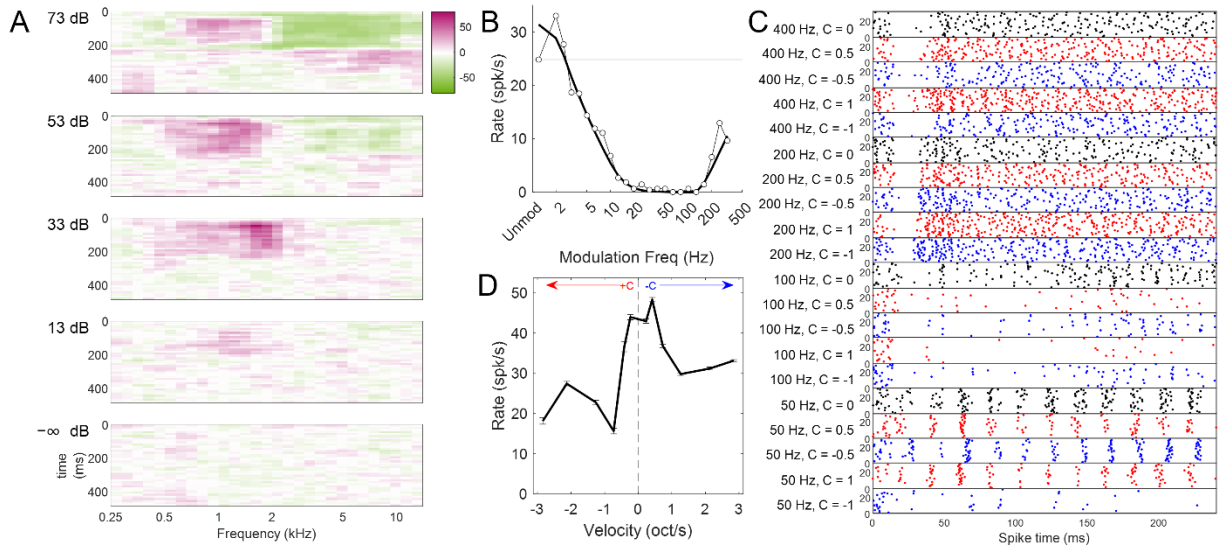

Figure 3 – Responses of unit R24TT4P7N2 to characterizing stimuli. (A) Response Map – Panels are arranged vertically by sound level of pure tones. Color plots reflect response rate versus frequency (abscissa) and time following tone onset (ordinate); magenta regions have increased activity relative to spontaneous rate, and green regions have decreased activity relative to spontaneous rate. (B) Modulation Transfer Function – rate versus modulation frequency. The solid black line is smoothed from raw data (shown as circular points). Grey horizontal line reflects unmodulated rate. (C) Dot rasters of SCHR responses – Panels are arranged vertically by SCHR condition (F0 and C-value pairs). Within panels, rows of dots reflect repetitions (30 each). Responses to negative C-values (-SCHR) are plotted with blue dots, and positive C-values (+SCHR) with red dots. Black is used for C = 0. (D) Rate-velocity function – constructed using responses to ARC-stimuli. Colored arrows mark the SCHR C-values of chirps of equivalent direction. Error bars are the standard error of rates across repetitions (20 each).

Another example neuron, illustrated in Fig. 4, had a BE MTF, and a RM dominated by excitation, with a CF of 2 kHz. Its SCHR raster showed relatively greater responses to +SCHR chirps for all chirp pairs, with the exception of 400-Hz SCHR stimuli, which were comparatively direction-neutral. Also notable is the suppressed response to 400-Hz SCHR relative to other F0s.

Figure 5 shows responses of an example neuron with a BE MTF and a RM similarly dominated by excitation, with a CF of 2.3 kHz. However, this neuron was –SCHR selective for nearly all chirp pairs, with the exception of 400-Hz SCHR. Thus, neurons with the same MTF type could have opposing chirp-direction selectivity. Again, the MTF shape alone did not predict SCHR responses. Additionally, neither of the neurons in Figs. 4 and 5 had RMs with inhibitory regions—there was also no evidence for inhibition from either ear based on the neurons' binaural noise response. The lack of inhibition in either neuron suggests that sideband inhibition was not strictly a requirement for chirp sensitivity. Finally, these neurons both had RVFs that were consistent with the SCHR rate profiles. In Fig. 4, downward-sweeping chirps elicited a higher response rate than upward-sweeping ones for every velocity-pair. In Fig. 5, the responses to upward-sweeping chirps were larger to all velocity-pairs, except for ±2.13 oct/ms (equivalent to 400 Hz)—interestingly, the selectivity for -SCHR seen for other SCHR conditions in the dot raster was absent for the 400-Hz pair.

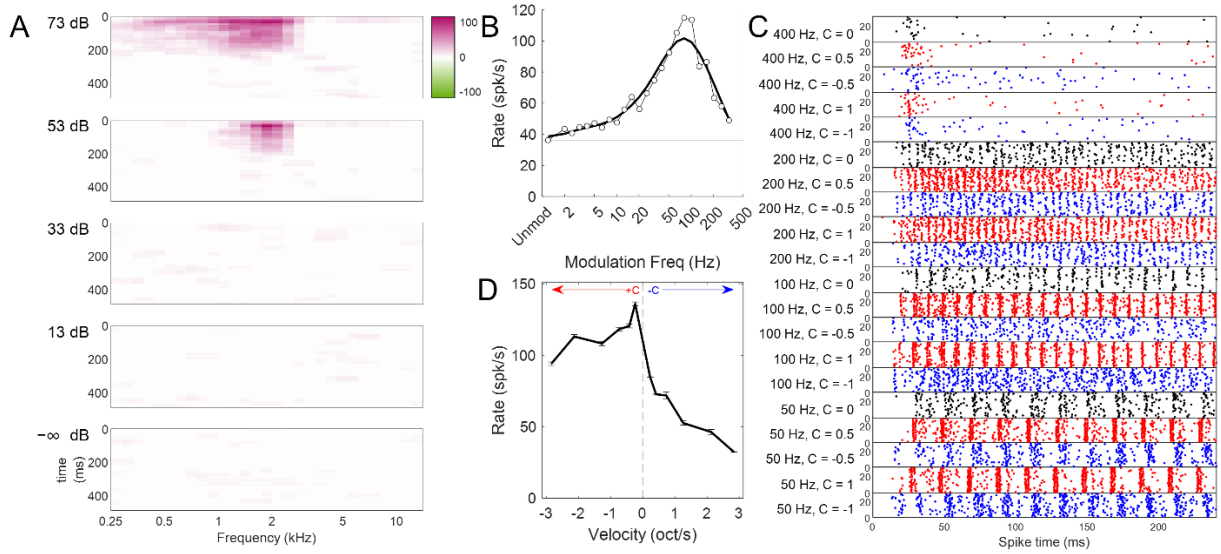

Figure 4 – Responses of unit R24TT2P8N4 to characterizing stimuli. (A) Response Map, (B) Modulation Transfer Function, (C) SCHR dot raster, (D) Rate-Velocity Function. Figure description identical to Fig. 3.

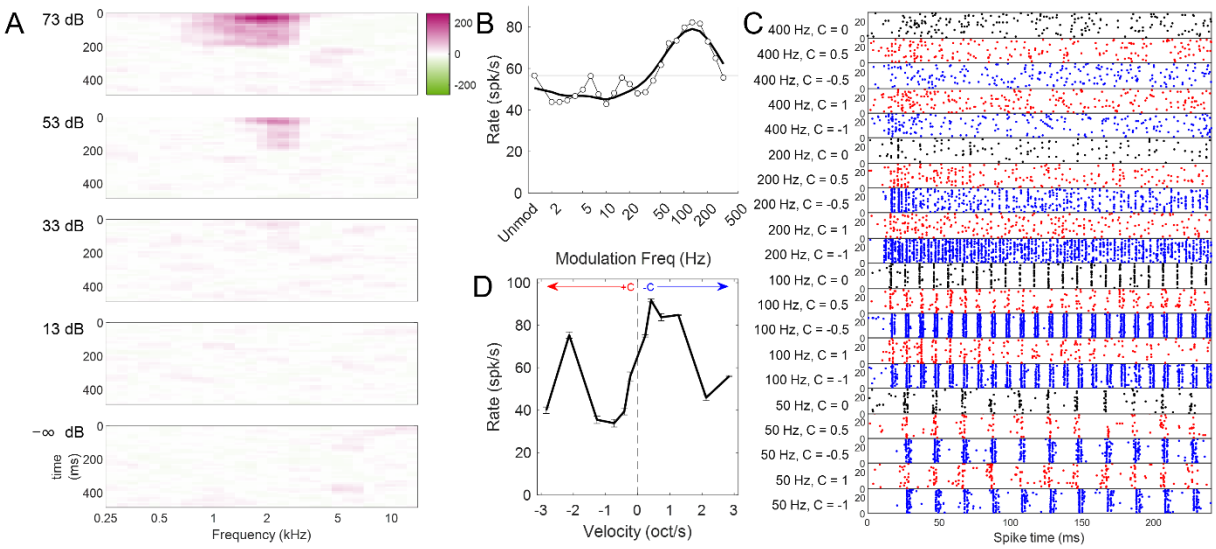

Figure 5 – Responses of unit R25TT2P5N1 to characterizing stimuli. (A) Response Map, (B) Modulation Transfer Function, (C) SCHR dot raster, (D) Rate-Velocity Function. Figure description identical to Fig. 3.

Figure 6 shows responses of a neuron with a flat MTF that was also selective for –SCHR chirps for low-F0 chirp pairs. This figure illustrates that neurons that were neither BE nor BS could still be sensitive to the direction of SCHR chirps, providing further evidence that SCHR sensitivity was not a property tied to a particular MTF type.

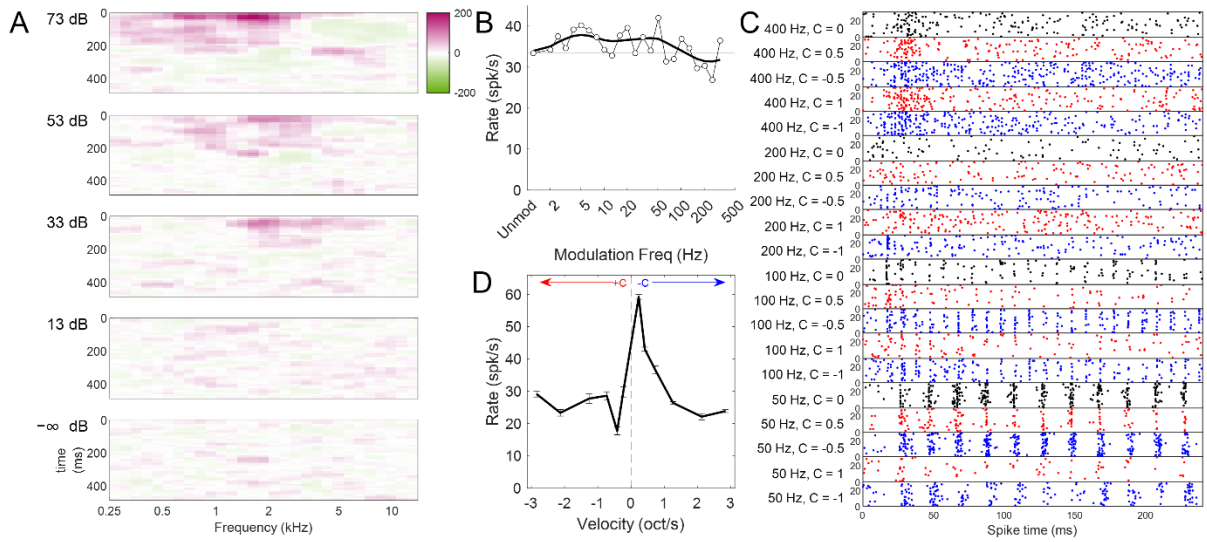

Figure 6 – Responses of unit R24TT2P8N3 to characterizing stimuli. (A) Response Map, (B) Modulation Transfer Function, (C) SCHR dot raster, (D) Rate-Velocity Function. Figure descriptions identical to Fig. 3.

Figure 7 shows responses of an example neuron with an RM that had a low-frequency inhibitory region at high tone levels. This low-frequency inhibitory sideband would predict a selectivity towards downward chirps (i.e., +SCHR), but the neuron's SCHR rasters show a selectivity towards upward chirps (–SCHR). Figures 3 and 7 are examples for which chirp selectivity did not agree with the prediction made by the asymmetric inhibitory sideband theory (Fuzessery & Hall, 1996; Gordon and O'Neill, 1998) and suggest that sideband inhibition alone could not predict SCHR responses.

Figure 7 – Responses of unit R24TT1P9N2 to characterizing stimuli. (A) Response Map, (B) Modulation Transfer

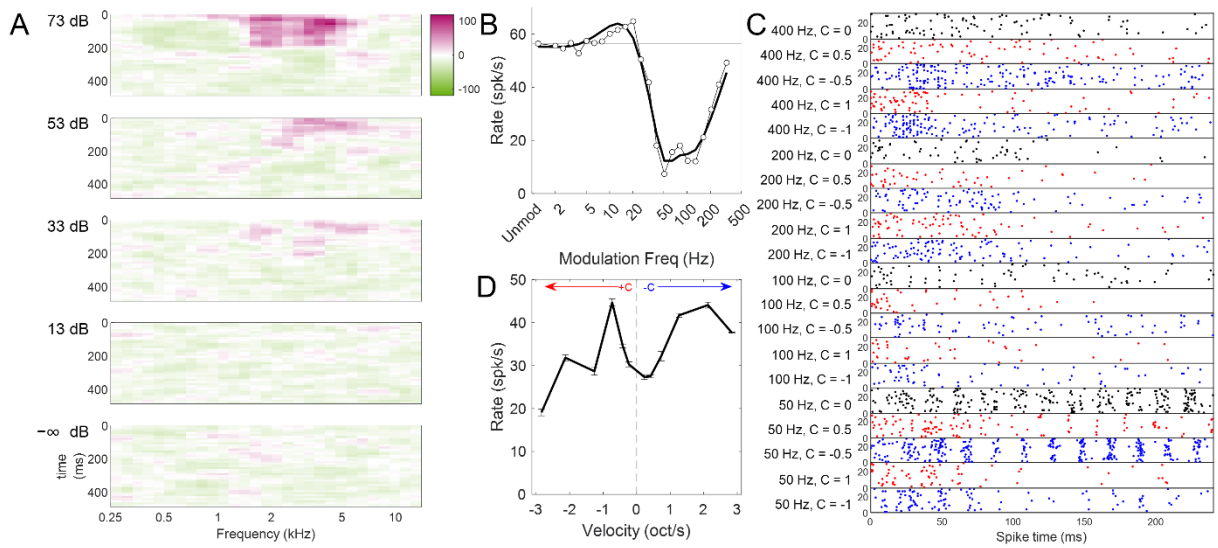

Function, (C) SCHR dot raster, (D) Rate-Velocity Function. Figure description identical to Fig. 3.

These example neurons illustrate the diversity of response profiles to SCHR chirps in the IC. Conventional IC feature sensitivities, such as modulation tuning and off-CF inhibition, could not fully explain the responses to SCHR chirps. This observation led to the hypothesis that sensitivity to the chirp velocity contributed to SCHR-chirp sensitivity. This hypothesis served as the motivation for the ARC stimulus, which allowed variation of the velocity cue. RVFs based on ARC-stimulus responses often reflected the rate profiles seen in SCHR dot rasters (e.g., Fig. 4,5,6), but sometimes did not (e.g., Fig 3,7), suggesting that while many neuron's SCHR responses could be explained by their RVFs, others required a more complex interaction between multiple feature sensitivities.

B. The majority of IC neurons were selective for SCHR direction

After establishing that individual IC neurons in awake rabbit displayed sensitivity for SCHR-chirp direction, this property was quantified for the full population of recorded neurons.

SCHR-direction sensitivity was quantified within a given F0 and pair of opposite-signed C values by performing ROC analysis on response rates for SCHR-sign pairs. SCHR-sign pairs for which direction could be discriminated 70.7% of the time via the ROC test were labeled direction-sensitive.

In total, SCHR responses were recorded from 157 neurons. In Table 1, the Overall column shows the percentage of all neurons that were direction selective for each F0 and C condition, or for at least one combination (i.e., Any). Direction selectivity was more common for lower F0s. Neurons were most commonly direction selective for the F0 = 50 Hz, C = ±0.5 condition and least commonly selective for the F0 = 200 Hz, C = ±0.5 condition.

F0 (Hz)	C-Value	Overall (n = 157)	BE (n = 31)	BS (n = 59)	Hybrid (n = 41)	Low CF (n = 36)	Mid CF (n = 39)	High CF (n = 82)
50	±1	53.5	74.2	45.8	51.2	58.3	61.5	47.6
	±0.5	59.2	81.0	47.1	60.0	56.7	73.9	55.6
100	±1	51.0	77.4	44.1	36.6	63.9	61.5	40.2
	±0.5	51.2	66.7	49.0	34.3	50.0	73.9	44.4
200	±1	50.3	67.7	47.5	36.6	63.9	56.4	41.5
	±0.5	35.2	71.4	23.5	22.9	33.3	60.9	27.8
400	±1	49.0	48.4	47.5	51.2	47.2	48.7	50.0
	±0.5	48.8	66.7	41.2	45.7	46.7	56.5	47.2
Any		**90.5**	**93.6**	**93.2**	**82.9**	**97.2**	**92.3**	**86.6**

Table 1 - Percent of direction sensitive neurons by subgroup as determined by ROC analysis of SCHR responses. Neurons are sorted into subgroups by MTF shape and CF. Neurons with CF less than 6 kHz were labeled "Low CF", and neurons with CF greater than 6 kHz were labeled "High CF". Direction sensitivity was quantified for each F0/C condition. The percentage of neurons sensitive for any F0/C condition was also determined, defined as neurons that were sensitive to sweep direction for at least one F0/C condition.

For a given F0, the C = ±0.5 condition had a chirp velocity equivalent to the 2F0 and C = ±1 condition. However, these equivalent-velocity pairs differed in prevalence of direction selectivity (i.e., 200 Hz, C = ±0.5 and 400 Hz, C = ±1, Overall column). This result suggested that prevalence of direction selectivity did not depend solely on chirp velocity, and was possibly also influenced by SCHR periodicity or duty cycle.

Finally, 90.5% of neurons were direction selective for at least one F0 and C condition (Table 1, *Any* row), demonstrating that SCHR chirp direction selectivity was nearly ubiquitous. To confirm that percentages in the *Any* row of Table 1 were not simply the result of increased response variance due to multiple comparisons, responses to either direction were shuffled within each SCHR-sign pair for each neuron. ROC tests were then performed on these shuffled responses, and the neurons that were direction selective for at least one F0/C condition were tallied as before. After shuffling the responses 1000 times, 3.2% of the neurons were selective for at least one F0/C condition (with a standard deviation of 2.6%), suggesting that the threshold used in the ROC test (70.07%) was sufficiently high.

C. MTF shape, but not CF, was related to prevalence and direction of SCHR selectivity

The prevalence of SCHR-direction selectivity depended on F0, hence it was relevant to determine whether prevalence of direction selectivity was related to MTF type. To examine the effect of MTF shape on SCHR direction selectivity, results of ROC analysis are shown in Fig. 8. BE neurons were significantly more direction selective than BS neurons for 5 SCHR conditions, and more direction selective than Hybrid neurons for 5 conditions, suggesting that BE neurons were more often direction selective than other MTF shapes (chi-square test of independence, $p < 0.05$). Additionally, for several SCHR conditions (e.g., 50 Hz, C = ±1; 50 Hz, C = ±0.5; 400 Hz, C = ±0.5) a notably larger percentage of BE neurons were +SCHR selective than for the rest of the MTF shapes, suggesting that BE neurons were more likely than neurons of other MTF types to be +SCHR selective. For most SCHR conditions, all MTF types tended to have more –SCHR selective neurons. However, for all but one MTF group and SCHR condition (Other, 50 Hz, C = ±50 Hz), both positively- and negatively-selective neurons appeared.

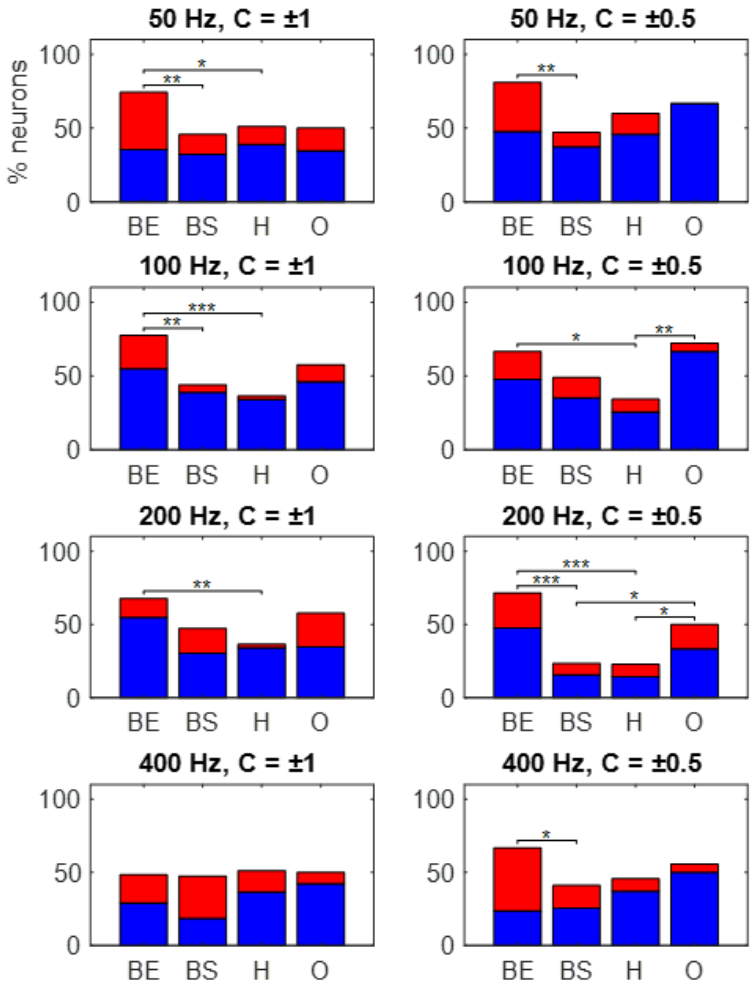

Figure 8 - Percent of direction selective neurons determined by ROC analysis for different MTF shapes, by SCHR condition (BE – Band-Enhanced, BS – Band-Suppressed, H – Hybrid, O – Other). Blue bar-segments correspond to – SCHR selective neurons, and red bar-segments correspond to +SCHR selective neurons. Brackets indicate significant differences of direction selectivity prevalence between groups, as determined by the chi-square test of independence, with asterisks indicating the level of significance ($p < 0.05$, ** $p < 0.01$, *** $p < 0.001$).*

Interestingly, despite the large differences between BE and BS groups within individual SCHR conditions, the percentage of neurons in each group that were direction selective at any SCHR condition (Table 1, bottom row) were similar. This result shows that BS neurons were

more frequently selective only at a few SCHR conditions compared to BE neurons. Indeed, the average number of selective SCHR conditions among BE neurons was 4.6, compared to 3.2 conditions on average for BS neurons. Hybrid neurons were selective for 3.1 conditions on average. Overall, direction selectivity prevalence among BE, BS, and hybrid neurons was high, with hybrid neurons having the lowest prevalence.

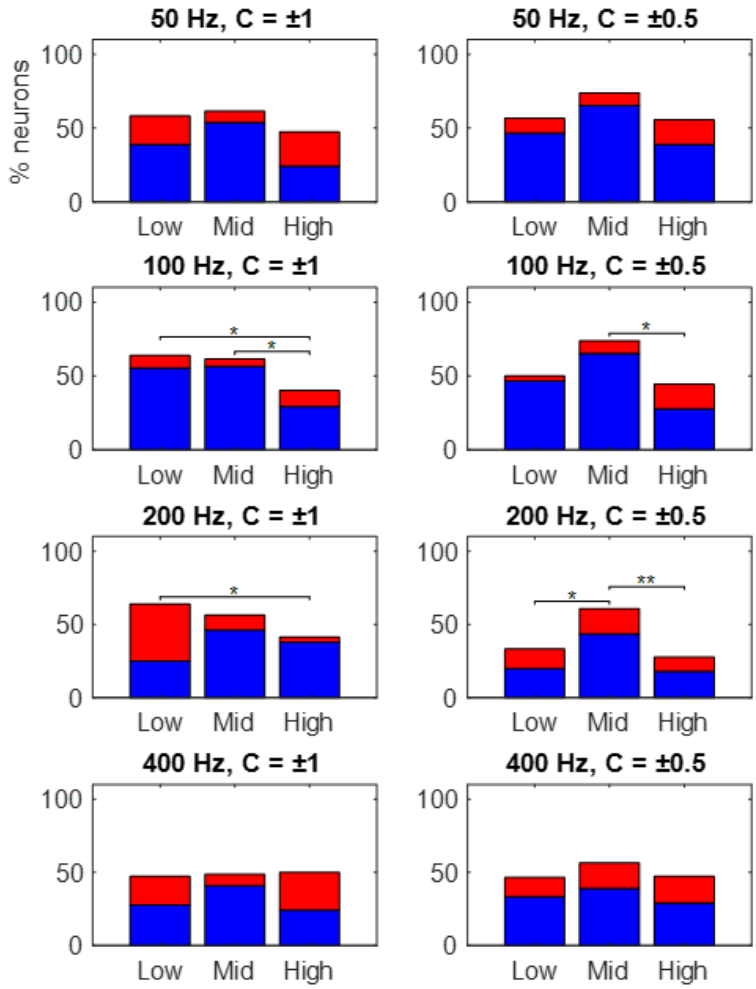

Figure 9 - Percent of direction selective neurons determined by ROC analysis for different CF ranges, low (<3 kHz), mid (>3 kHz and <6 kHz), and high (>6 kHz), by SCHR condition. Blue bar-segments correspond to –SCHR selective neurons, and red bar-segments correspond to +SCHR selective neurons. Brackets indicate significant differences of

direction selectivity prevalence between groups, as determined by the chi-square test of independence, with asterisks indicating the level of significance (p < 0.05, ** p < 0.01, *** p < 0.001).*

To examine the effect of CF on SCHR direction selectivity, results of ROC analysis for different CF ranges are shown in Fig. 9. The relationship of prevalence of selectivity and CF is less clear than for MTF shape. Generally, low-CF and mid-CF neurons were more often selective than high-CF neurons, but this trend varied by SCHR condition. Generally, most CF groups had more –SCHR selective neurons for all SCHR conditions. Generally, mid-CF neurons displayed robust –SCHR selectivity compared to high-CF neurons, which were more +SCHR selective. Low-CF neurons may have been more selective for –SCHR at low F0s, but become more balanced at higher F0s. Overall, much like MTF groups, all CF groups had both positive- and negative-selective neurons. Also, like the MTF groups, all CF groups had an overall high percentage of direction selectivity (Table 1, *Any* row).

D. Direction selectivity to ARC stimuli was near-ubiquitous

Velocity (oct/ms)	Overall (n = 247)	BE (n = 33)	BS (n = 115)	Hybrid (n = 67)	Low CF (n = 90)	Mid CF (n = 36)	High CF (n = 121)
0.23	80.2	90.9	80.9	71.6	85.6	86.1	74.4
0.42	72.9	78.8	72.2	67.2	78.9	69.4	69.4
0.73	73.3	87.9	73.9	73.1	76.7	75.0	70.2
1.26	62.3	69.7	53.9	71.6	57.8	55.6	67.8
2.13	56.3	63.6	53.9	61.2	53.3	38.9	63.6
2.84	52.2	48.5	47.8	61.2	46.7	52.8	56.2
Any	**99.6**	**100**	**100**	**98.5**	**100**	**100**	**99.2**

Table 2 – Percent of direction selective neurons by subgroup as determined by ROC analysis of ARC-stimulus responses. Neurons are sorted into subgroups by MTF shape and CF. Neurons with CF less than 6 kHz were labeled "Low CF", and neurons with CF greater than 6 kHz were labeled "High CF". Direction selectivity was quantified for each F0/C condition. The percentage of neurons selective for any F0/C condition was also determined, defined as neurons for which at least one F0/C condition was selective.

ROC analysis was performed on responses to ARC stimuli to determine the prevalence of direction selectivity of neurons in the absence of periodicity. Similar to the analysis performed

for SCHR responses (Table 1), equivalent ARC chirp speeds were paired, and pairs for which the chirp direction could be discriminated 70.7% of the time via ROC test were labeled direction-selective.

ARC responses were collected from 247 neurons (Table 2). Like the SCHR ROC results, direction selectivity to ARC stimuli was common for faster chirp velocities and became increasingly uncommon for higher velocities. When comparing equivalent chirp-velocity conditions between SCHR and ARC-stimulus responses (e.g., 0.42 oct/ms ARC chirp and 50-Hz SCHR, etc.), neurons were more commonly selective for ARC chirps than for their SCHR counterparts. Finally, 99.6% of neurons were direction selective for at least one ARC velocity (Table 2, *Any* row). Stated differently, only one neuron among the 247 surveyed was not direction selective at any velocity. This result demonstrates that neurons were nearly universally direction selective to chirps in aperiodic stimuli.

As was done with the SCHR ROC analysis, responses to each chirp-direction pair were shuffled for each neuron, and an ROC test was performed on the shuffled responses to ensure that a reasonable threshold was used for determining direction selectivity. Shuffling the responses 1000 times, 13.3% of the neurons were selective for at least one F0/C condition (with a standard deviation of 9.0%). It is clear that the actual percentage of 99.6% could not be due to variance in the data, suggesting that the threshold used in the ROC test (70.07%) was sufficiently high.

E. Prevalence and direction of ARC selectivity were related to chirp velocity, but not MTF shape or CF

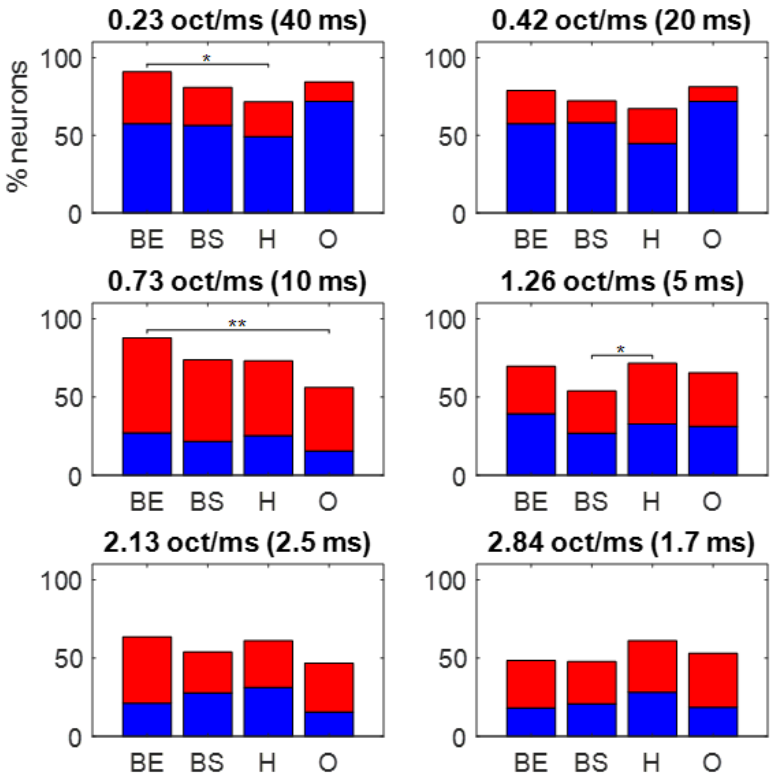

Figure 10 - Percent of direction selective neurons determined by ROC analysis for different MTF shapes, by ARC chirp duration (BE – Band-Enhanced, BS – Band-Suppressed, H – Hybrid, O – Other). In terms of chirp velocity, an ARC chirp of 0.42 oct/ms has a duration of 20 ms (equivalent to a SCHR chirp F0 of 50 Hz), 0.73 oct/ms has a duration of 10 ms (SCHR F0 100 Hz, etc.). Blue bar-segments correspond to upward-selective neurons (equivalent to -SCHR), and red bar-segments correspond to downward-selective neurons (equivalent to +SCHR). Brackets indicate significant differences of direction selectivity prevalence between groups, as determined by the chi-square test of independence, with asterisks indicating the level of significance ($p < 0.05$, ** $p < 0.01$, *** $p < 0.001$).*

The results of ROC analysis revealed different trends for ARC responses than responses to SCHR. There was not as pronounced of an effect of MTF shape on either the

prevalence or direction of ARC selectivity (Fig. 10). BE-neuron selectivity was not more prevalent than that of other MTF shapes, as seen in Fig. 8. Instead, all MTF shapes showed decreasing prevalence of direction selectivity with increasing chirp velocity (Table 2). Direction of ARC selectivity changed with chirp velocity as well – at the two slower velocities tested (0.23 and 0.42 oct/ms), neurons were more frequently selective for positive chirp velocities (blue, equivalent to -SCHR). At the four higher velocities (0.73 oct/ms and faster), neurons of all MTF types were more likely to be selective for negative velocities (red, equivalent to +SCHR).

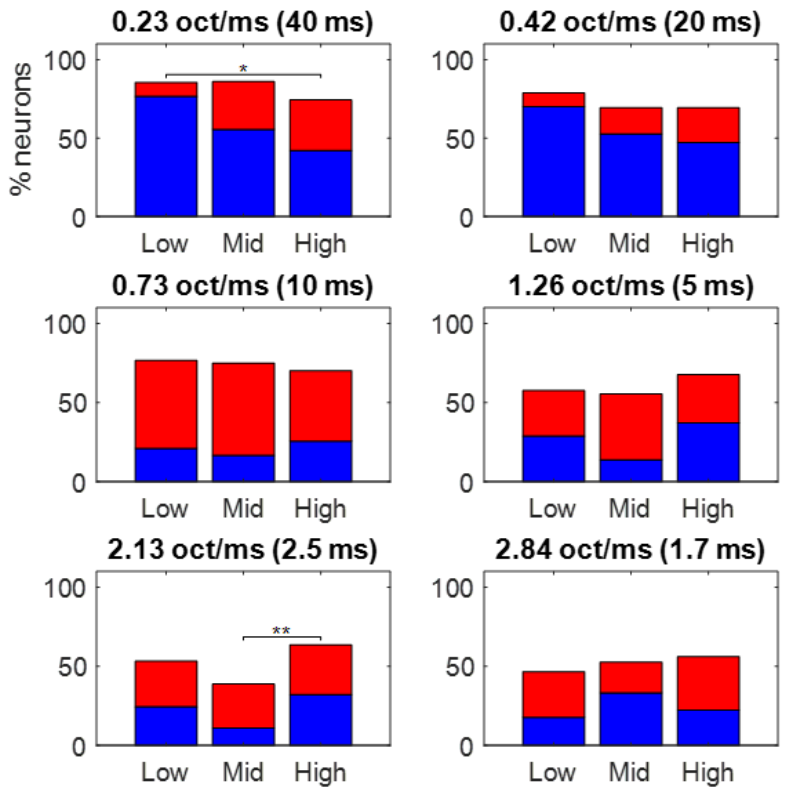

Figure 11 - Percent of direction selective neurons determined by ROC analysis for different CF ranges, low (<3 kHz), mid (>3 kHz and <6 kHz), and high (>6 kHz), by ARC chirp. In terms of chirp velocity, an ARC chirp of 0.42 oct/ms has a duration of 20 ms (equivalent to a SCHR chirp F0 of 50 Hz), 0.73 oct/ms has a duration of 10 ms (SCHR F0 100 Hz, etc.). Blue bar-segments correspond to upward-selective neurons (equivalent to -SCHR), and red bar-segments correspond to downward-selective neurons (equivalent to +SCHR). Brackets indicate significant differences of

direction selectivity prevalence between groups, as determined by the chi-square test of independence, with asterisks indicating the level of significance ($p < 0.05$, ** $p < 0.01$, *** $p < 0.001$).*

The trends observed for direction selectivity in neurons with different MTF types were also observed for CF groups (Fig. 11). CF was not strongly related to the prevalence nor the direction of ARC selectivity; rather, prevalence of direction sensitivity in all CF groups decreased with increasing chirp velocity. Also, neurons were more commonly selective for chirps of negative velocity (+SCHR) at higher chirp velocities.

F. Neurons' RVFs were often direction selective at slower-velocities and direction-insensitive at higher-velocities

In order to determine which response properties were the most common, principal component analysis (PCA) was performed on the set of RVFs. Figure 12 shows the first three principal components, which together explained 74.0% of the variance in the data. Principal component 1 (PC1) had relatively high weights at high-magnitude velocities, showing that rate responses to high velocities tended to be positively correlated, regardless of direction. PC1 explained 48.5% of variance in the RVF data. Principal component 2 (PC2) had high weights at low-magnitude velocities, showing that rate responses to low velocities also tended to be positively correlated, regardless of direction. PC2 explained 13.8% of variance in the data. Finally, PC3 had large positive weights at positive, slow velocities and negative weights at negative, slow velocities, demonstrating that positive and negative velocity chirps tended to be negatively correlated at slow velocities. PC3 appeared to be the main PCA dimension reflecting direction selectivity. PC3 explained 11.7% of variance in the data.

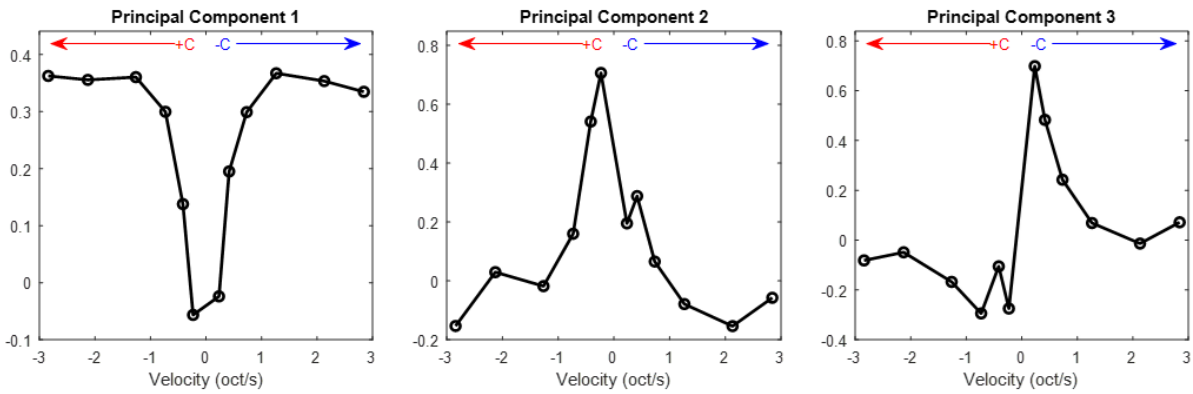

Figure 12 – Principal components derived from the set of RVFs (left, PC1; center, PC2; right, PC3). Y-axes reflect principal-component weights and are unitless.

The shapes of the first three principal components of the RVF data suggest that the most salient features of a neuron's RVF were its responses to high- and low-velocity chirps, rather than the direction of those chirps. However, PC3 showed that the direction selectivity of neurons for low-velocity chirps was an important feature of these datasets—however, PC3 primarily represented low-velocity chirp direction selectivity, suggesting that chirp-direction selectivity at high-velocities was not as common; instead, a neuron's response to chirps of high velocities tended to depend on the absolute velocity rather than on its direction.

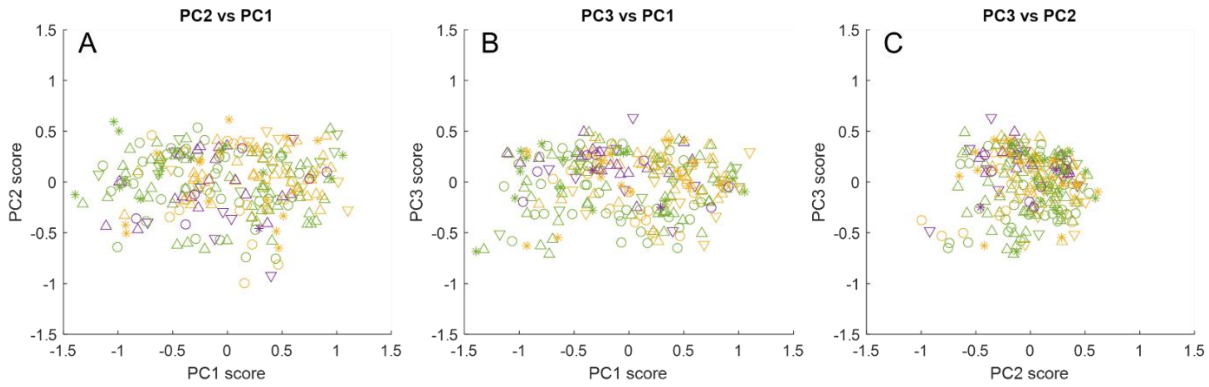

Figure 13 – Scatter plots depicting the Principal Component scores of each neuron (A, PC2 vs PC1; B, PC3 vs PC1; C, PC3 vs PC2). MTF shape is denoted by marker shape (BE neurons are represented by upward triangles, BS neurons by downward triangles, hybrid neurons by circles, and other MTF shapes by asterisks). CF is denoted by color (Low CF neurons are represented by yellow points, mid CF by purple points, and high CF by green points).

As shown in Fig. 13, there was not a clear relationship between the scores of principal components 1-3 and either MTF type (symbol shapes) or CF (symbol colors). This result suggested that RVFs could not be simply derived from MTFs or CFs. Furthermore, based on the three scatter plots in Fig. 13, there were no clusters of neurons based on principal-component analysis – that is, RVF subgroups were not revealed by this analysis.

G. Velocity cues facilitated predictions of SCHR rate

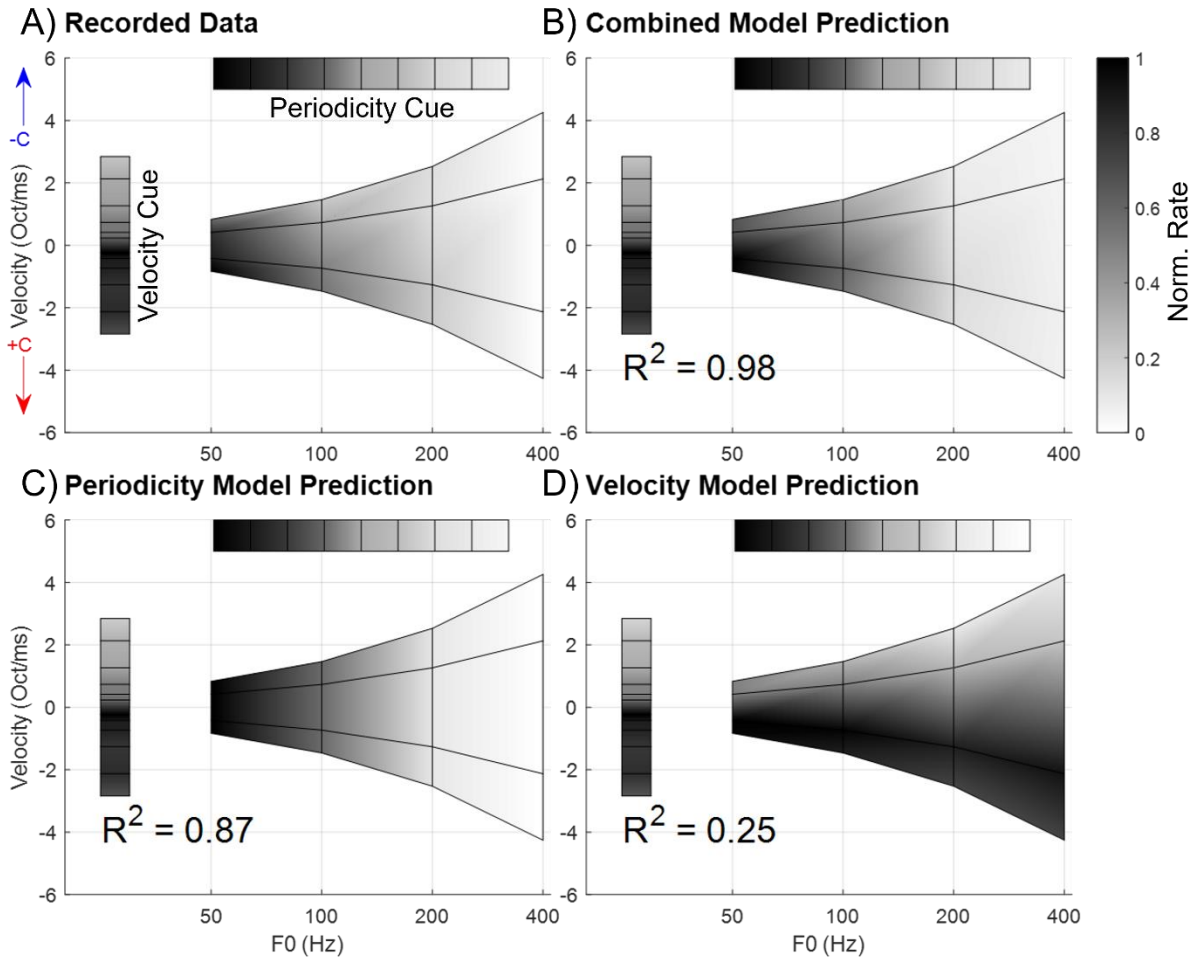

Figure 14 – GLM prediction of SCHR rates for an example neuron (R24TT2P8N4). (A) SCHR rates plotted in Periodicity-Velocity space (center surface). Each of the 16 points on the surface plot correspond to an individual SCHR F0/C-value combination – for instance, four points have a SCHR F0 of 50 Hz. Their velocities vary with C-value; the points' C-values, from top to bottom, are -0.5, -1, 1, 0.5. This surface plot demonstrates the effect of C-value on chirp velocity. The periodicity cue and velocity cue are plotted alongside the SCHR surface plot—these are the MTF and RVF, respectively. The modulation frequency range of the MTF was limited to the section relevant to the range of SCHR F0s (50 – 400 Hz). Rate is marked using color, with darker shades indicating larger rates. The rate scale of each surface plot is separately normalized by its own maximum rate—thus, shading does not reflect absolute rates. Surface plot colors are interpolated. (B) SCHR rates predicted using the combined GLM equation (Eqn. 1), which

uses periodicity and velocity cues. Coefficient of determination (R^2) between predicted and recorded SCHR rates is also shown. (C) SCHR rates predicted using the periodicity-only GLM equation (Eqn. 2), and corresponding R^2-value. (D) SCHR rates predicted using the velocity-only GLM equation (Eqn. 3), and corresponding R^2-value.

Starting from the premise that responses to SCHR stimuli are dependent on AM (periodicity) tuning and/or velocity tuning, we used MTFs and ARC responses to predict SCHR responses using the GLM. Figure 14 shows a visualization of this strategy on an example neuron. The neuron's SCHR response is shown as a surface plot on periodicity-velocity axes; darker colors correspond to higher response rates. This neuron responded more strongly to lower F0s and to +SCHR (Fig. 14A). The color bars above and to the left of the SCHR surface are the MTFN and ARC responses of the neuron, respectively, and describe how the neuron's response rate depended on periodicity or velocity alone. Using a weighted combination of these two responses, the GLM predicted the SCHR response (Fig. 14B). By fitting an equation that included both periodicity and velocity terms (Eqn. 1), an accurate prediction of the recorded SCHR data was made ($R^2 = 0.98$). Removing either the periodicity or velocity terms reduced the quality of the prediction (Fig. 14C, D) (note that their interaction will be examined below). Predicting the SCHR response using the periodicity-only model (Eqn. 2) resulted in the disappearance of the distinct direction selectivity at lower F0s (Fig. 14C). Notably, a model using only periodicity tuning could not explain the observed direction selectivity. Conversely, a prediction of the SCHR responses using the velocity-only model (Eqn. 3) explained a relatively small amount of variance in the data ($R^2 = 0.25$). This neuron was typical in that more variance in the data was explained by the periodicity-only model than by the velocity-only model. However, this neuron was also typical in that the velocity terms contribute a substantial percentage of the variance explained by the combined model, as compared to the periodicity-only model.

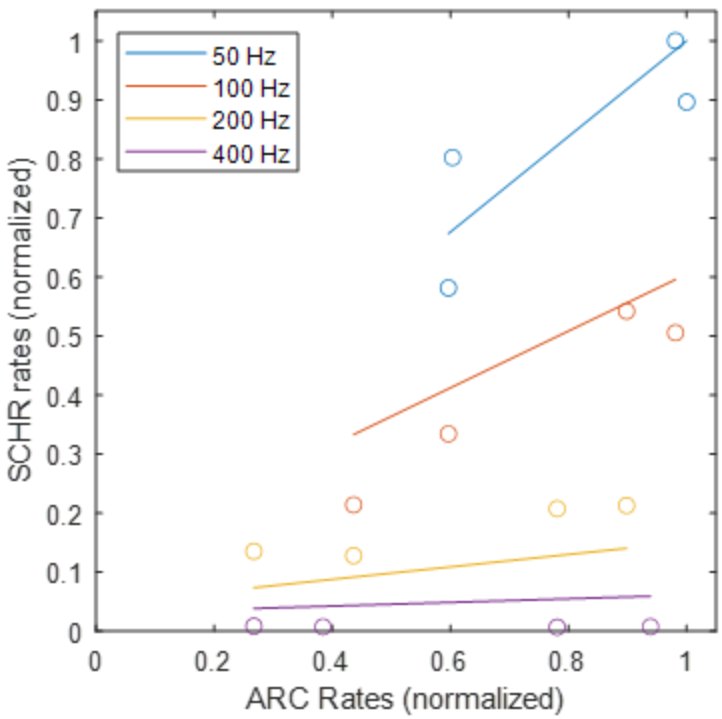

Figure 15 – SCHR rates vs ARC rates (velocity cue) of unit R24TT2P8N4 plotted as recorded data (scatter plot) and GLM-fitted lines (solid lines). Data are organized into groups of equivalent F0s by color. Both SCHR and ARC rates are normalized by their own maximum rate.

The example neuron in Fig. 14 had an RVF that showed a higher response rate for downward sweeps (+SCHR). However, this neuron's +SCHR selectivity was only seen at low F0s. Figure 15 shows how the velocity cue was used differently by the combined GLM model depending on periodicity. For ARC velocities that closely matched the velocities of 50-Hz-F0 SCHR chirps, a large change in ARC rate was associated with a high predicted SCHR rate (blue line). For higher F0s, ARC rate had less of an impact on predicted SCHR rate, SCHR-ARC-line slopes approaching zero (200 Hz and 400 Hz lines, yellow and purple). Therefore, despite the RVF suggesting a strong selectivity for downward sweeps at all velocities, Fig. 15 shows that the interaction between velocity and periodicity drove SCHR rates. The importance of velocity-periodicity interaction was typical across the sample of neurons surveyed.

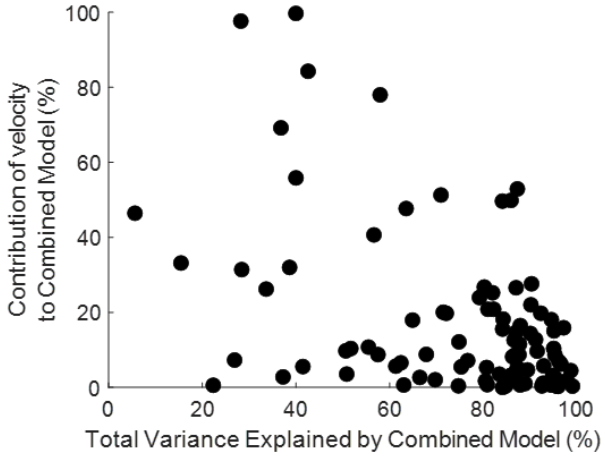

Figure 16 - A. (left) Percent variance explained in the SCHR response using the ARC model alone versus percent variance explained by the combined model. B. (right) Percent contribution of the ARC terms to the total explainable variance by the combined model vs. Variance explained by the combined model.

Using the method outlined in Figure 14, an R^2 value was obtained for each of the three GLM models (Eqns. 2-4) by comparing predictions to neural responses. The contribution of velocity terms to the total explainable variance was calculated as a percentage using Eqn. 4. Figure 16 shows this percentage versus variance explained by the combined model. Many symbols are clustered around the x-axis, indicating that the contribution of velocity was not the primary determinant of SCHR rate for many neurons. For these neurons, this result suggests that periodicity tuning is the more important feature in predicting SCHR response. However, for neurons with a high total explainable variance by the combined model (80-100%), the average contribution of velocity was about 20%. Figure 14 shows an example of such a neuron; the relatively small contribution by velocity was not insubstantial, and contained all information about direction selectivity, a cue for which the example unit was clearly sensitive (Fig. 4D, RVF). Furthermore, for many neurons with relatively low (20-60%) total explainable variance, the contribution of the velocity terms explained over 50% of the explained variance, suggesting that

velocity cues were important predictors of these neurons' SCHR responses, perhaps more so than the relatively weaker periodicity predictor.

In summary, direction selectivity between SCHR pairs could not be explained with a model using periodicity alone. Because SCHR-direction selectivity was common (90.5%, Table 1), most IC neuron responses were necessarily influenced by velocity sensitivity.

Discussion

This study demonstrated the diversity of sensitivity to the velocity and direction of fast frequency chirps in the IC, for the first time in an awake rabbit model. Using ROC analysis, IC neurons were shown to be commonly selective for SCHR chirp direction, with 90.5% of neurons surveyed selective for at least one condition (Table 1). Neurons were also nearly universally selective for chirp direction in response to the novel ARC stimulus (Table 2). This study also showed that individual neurons had a wide variety of rate-response profiles which could be described using RVFs. RVFs revealed that neurons were more commonly direction selective to chirps of lower velocities, and responded to higher velocities in a direction-insensitive way. Finally, GLM analysis was performed to show that in many cases SCHR rates could be accurately reconstructed using the periodicity and velocity sensitivity reflected in MTFs and RVFs, respectively. The combination of both velocity and periodicity cues was necessary to achieve the best model fits.

A common use of Schroeder-stimuli has been as a masker in tone-in-noise psychophysical experiments. Notably, there is an effect of Schroeder-phase on its effectiveness as a masker, with +SCHR maskers having up to 23-dB lower thresholds (less masking) than -SCHR maskers (Smith et al., 1986). An explanation from the literature attributes this effect to asymmetry of filtering in the cochlea—phase-dispersive properties of the basilar membrane (BM) result in a peakier response profile for +SCHR than -SCHR, which is then compressed at

the output of the cochlea, resulting in a larger response amplitude for -SCHR compared to +SCHR and more effective masking (Recio & Rhode, 2000; Summers et al., 2003). This logic could conceivably be applied to explain rate-differences between SCHR C-values in the IC. However, there are inconsistencies which suggest that other factors underlie the widespread chirp selectivity of IC single-units observed in this study. First, the phase-dispersion of the BM depends on CF, with masking differences observed primarily for neurons with CF > 3-4 kHz (Recio, 2001). In this study, no consistent differences were observed in either the prevalence or direction of chirp selectivity between low-CF (< 3 kHz) and mid- or high-CF (> 3 kHz) neurons, in either SCHR or ARC rates (Fig 9, 11). Furthermore, neurons in the CF range of the direction-selective cue observed in BM responses (> 3 kHz) were not uniformly selective for -SCHR (Fig. 9), suggesting other mechanisms must have shaped chirp selectivity.

A potential mechanism to explain the diverse chirp-response profiles seen in this study may be found in IC inhibition. IC neurons receive excitatory and inhibitory inputs with varying frequencies and latencies that may interact to produce chirp selectivity (Pollak et al., 2010). Interactions between excitatory and inhibitory inputs varying in latency have long been implicated in mechanisms for frequency-sweep selectivity in bats (Suga, 1965; Fuzessery & Hall, 1996; Gordon and O'Neill, 1998). These mechanisms broadly are dependent on sideband inhibitory regions in excitatory tuning curves and the resulting asymmetry of responses to upward and downward frequency sweeps. It is difficult to evaluate the specific applicability of these models to rabbit IC, since our study did not measure sideband inhibition directly; however, for many neurons (e.g., Fig. 4, 5), the absence of inhibition in binaural noise responses suggests that inhibition at the level of the IC is not a strict requirement for chirp-direction selectivity.

A related mechanism for chirp selectivity based on dendritic filtering was proposed by Rall (1969)—here, excitatory inputs are organized spatially by frequency. During a frequency

sweep, a sweep that activates distal dendrites first, and proximal dendrites later, would temporally sum and generate a large synaptic input. While the existence of such large dendritic fields has not been reported in the IC, this is the mechanism purported to underlie the FM directionality of octopus cells in the posteroventral cochlear nucleus (PVCN) (Rhode & Greenberg, 1992; Pollak et al., 2011). Notably, octopus cells project to the ventral nucleus of the lateral lemniscus (VNLL), which provides inhibitory innervation to the IC (Adams, 1997; Vater et al., 1997; Winer et al., 1995). Thus, FM directionality of octopus cells by way of the VNLL may explain chirp selectivity in the IC; in this scenario, responses to chirps of one direction would be inhibited by input from the VNLL and disinhibited by the opposite direction. The possibility that IC chirp sensitivity originates in octopus cells is particularly attractive because, like IC neurons, octopus cells display a diversity of chirp response profiles and can be selective to either upward or downward chirps (Lu et al., 2022).

Sensitivity to the direction of fast frequency changes has also been evaluated using neural response to high-velocity spectrotemporal fluctuations. One example is the Dynamic Moving Ripple (DMR) stimulus described in Escabi and Schreiner (2002). Designed to mimic spectrotemporal modulations present in natural sounds such as speech or animal vocalizations, the stimulus is composed of a bank of sinusoidal carriers with an imposed spectrotemporal envelope. This stimulus has been used to generate spectrotemporal receptive fields (STRFs), which describe how neural response properties vary over frequency and time. The stimulus works well to identify neurons' sensitivity to slower frequency modulations, but is not able to generate chirps of equivalent velocity to those found in SCHR stimuli. The ripple velocity of the DMR stimulus is roughly controlled by an instantaneous modulation frequency random variable Fm (i.e., frequency of the imposed envelope). In the original study, this variable had an upper bound of 350 Hz; meanwhile, in order to achieve an equivalent velocity to the SCHR chirps used in this study, this upper bound would have to increase to beyond 5000 Hz. However, this

frequency would far outstrip the limit of phase locking in the inferior colliculus (Kuwada, year), rendering the DMR stimulus ineffective at describing response properties to chirps of this speed. This limitation of the DMR stimulus further highlights a benefit of the SCHR stimulus – SCHR chirps are both “fast” in the velocity sense, and “slow” in the phase-locking sense, with F0s low enough for consistent phase-locked responses of IC neurons.

While the combined GLM with both periodicity and velocity cues was able to reproduce SCHR rate profiles of IC neurons, often with high accuracy, many predictions did not explain a high percentage of the variance (Fig. 16), suggesting that additional factors shaping SCHR rate profiles have yet to be uncovered. One possible source of this discrepancy was a gradual change in rate over long (50 – 150 ms) durations—Fig. 3 shows an example where rate gradually increased (100 Hz F0), and Fig. 7 shows an example where rate gradually decreased (50 Hz F0, C = -1). These long-term effects may be attributable to the auditory efferent system, and cannot be captured using the brief ARC stimulus. Similar long-term changes in rate have been reported in response to modulated noise stimuli, suggesting that the two may share a common mechanism (Farhadi et al., 2021).

SCHR-chirp sensitivity in the IC suggests a mechanism that may influence midbrain-level encoding of speech. When speech sounds, or any animal vocalizations, are produced, resonances within the vocal tract act as second-order filters, introducing phase shifts between components of harmonic sounds (Klatt, 1980). In the same way that SCHR chirps are produced by the relative phases of harmonic components, vocalizations will contain chirp-like features to which IC neurons may be similarly sensitive. IC neurons in this study were sensitive to SCHR chirps and directions over a frequency range relevant to human speech. Close examination of IC responses to SCHR chirps may reveal a novel influence on midbrain responses that is relevant to neural coding of speech and other harmonic sounds. The interaction of periodicity

tuning and frequency-sweep velocity sensitivity observed in this study would also influence responses to other complex harmonic sounds, such as those common in speech and music.

Acknowledgement Supported by NIDCD-R01-001641.

References

Andoni, S., Li, N., & Pollak, G. D. (2007). Spectrotemporal Receptive Fields in the Inferior Colliculus Revealing Selectivity for Spectral Motion in Conspecific Vocalizations. The Journal of Neuroscience, 27(18), 4882-4893. doi:10.1523/jneurosci.4342-06.2007

Awan, S. N., Novaleski, C. K., & Rousseau, B. (2014). Nonlinear Analyses of Elicited Modal, Raised, and Pressed Rabbit Phonation. Journal of Voice, 28(5), 538-547. doi:https://doi.org/10.1016/j.jvoice.2014.01.015

Caspary, D. M., Palombi, P. S., & Hughes, L. F. (2002). GABAergic inputs shape responses to amplitude modulated stimuli in the inferior colliculus. Hearing research, 168(1), 163-173. doi:https://doi.org/10.1016/S0378-5955(02)00363-5

Casseday, J. H., Ehrlich, D., & Covey, E. (1994). Neural Tuning for Sound Duration: Role of Inhibitory Mechanisms in the Inferior Colliculus. Science, 264(5160), 847-850. doi:10.1126/science.8171341

Davis, K. A. (2005). Spectral Processing in the Inferior Colliculus. In International Review of Neurobiology (Vol. 70, pp. 169-205): Academic Press.

Escabi, M. A., Miller, L. M., Read, H. L., & Schreiner, C. E. (2003). Naturalistic auditory contrast improves spectrotemporal coding in the cat inferior colliculus. Journal of Neuroscience, 23(37), 11489-11504.

Escabi, M. A., & Schreiner, C. E. (2002). Nonlinear spectrotemporal sound analysis by neurons in the auditory midbrain. Journal of Neuroscience, 22(10), 4114-4131.

Fuzessery, Z., & Hall, J. (1996). Role of GABA in shaping frequency tuning and creating FM sweep selectivity in the inferior colliculus. Journal of Neurophysiology, 76(2), 1059-1073.

Fuzessery, Z. M. (1994). Response selectivity for multiple dimensions of frequency sweeps in the pallid bat inferior colliculus. Journal of Neurophysiology, 72(3), 1061-1079. doi:10.1152/jn.1994.72.3.1061

Geis, R., & Borst, G. (2013). Intracellular responses to frequency modulated tones in the dorsal cortex of the mouse inferior colliculus. Frontiers in Neural Circuits, 7. doi:10.3389/fncir.2013.00007

Gordon, M., & O'Neill, W. E. (1998). Temporal processing across frequency channels by FM selective auditory neurons can account for FM rate selectivity. Hearing research, 122(1-2), 97-108.

Hage, S. R., & Ehret, G. (2003). Mapping responses to frequency sweeps and tones in the inferior colliculus of house mice. European Journal of Neuroscience, 18(8), 2301-2312. doi:https://doi.org/10.1046/j.1460-9568.2003.02945.x

Heffner, H., & Masterton, B. (1980). Hearing in Glires: Domestic rabbit, cotton rat, feral house mouse, and kangaroo rat. The Journal of the Acoustical Society of America, 68(6), 1584-1599. doi:10.1121/1.385213

Kim, D. O., Carney, L., & Kuwada, S. (2020). Amplitude modulation transfer functions reveal opposing populations within both the inferior colliculus and medial geniculate body. Journal of Neurophysiology, 124(4), 1198-1215. doi:10.1152/jn.00279.2020

Klatt, D. H. (1980). Software for a cascade/parallel formant synthesizer. The Journal of the Acoustical Society of America, 67(3), 971-995. doi:10.1121/1.383940

Koch, U., & Grothe, B. (1998). GABAergic and Glycinergic Inhibition Sharpens Tuning for Frequency Modulations in the Inferior Colliculus of the Big Brown Bat. Journal of Neurophysiology, 80(1), 71-82. doi:10.1152/jn.1998.80.1.71

Krips, R., & Furst, M. (2009). Stochastic properties of coincidence-detector neural cells. Neural computation, 21(9), 2524-2553.

Krishna, B. S., & Semple, M. N. (2000). Auditory Temporal Processing: Responses to Sinusoidally Amplitude-Modulated Tones in the Inferior Colliculus. Journal of Neurophysiology, 84(1), 255-273. doi:10.1152/jn.2000.84.1.255

Kuwada, S., Stanford, T. R., & Batra, R. (1987). Interaural phase-sensitive units in the inferior colliculus of the unanesthetized rabbit: effects of changing frequency. Journal of Neurophysiology, 57(5), 1338-1360. doi:10.1152/jn.1987.57.5.1338

Li, A.-A., Zhang, A.-Y., Chen, Q.-C., & Wu, F.-J. (2010). Effects of modulation range and presentation rate of FM stimulus on auditory response properties of mouse inferior collicular neurons. Sheng li xue bao : [Acta physiologica Sinica], 62(3), 210-218. Retrieved from http://europepmc.org/abstract/MED/20571737

Nelson, P. C., & Carney, L. H. (2007). Neural Rate and Timing Cues for Detection and Discrimination of Amplitude-Modulated Tones in the Awake Rabbit Inferior Colliculus. Journal of Neurophysiology, 97(1), 522-539. doi:10.1152/jn.00776.2006

Pollak, G. D., Xie, R., Gittelman, J. X., Andoni, S., & Li, N. (2011). The dominance of inhibition in the inferior colliculus. Hearing research, 274(1), 27-39. doi:https://doi.org/10.1016/j.heares.2010.05.010

Poon, P. W., Chen, X., & Cheung, Y. (1992). Differences in FM response correlate with morphology of neurons in the rat inferior colliculus. Experimental brain research, 91(1), 94-104.

Schroeder, M. (1970). Synthesis of low-peak-factor signals and binary sequences with low autocorrelation (Corresp.). IEEE Transactions on Information Theory, 16(1), 85-89.

Schwarz, D. M., Zilany, M. S. A., Skevington, M., Huang, N. J., Flynn, B. C., & Carney, L. H. (2012). Semi-supervised spike sorting using pattern matching and a scaled Mahalanobis

distance metric. Journal of Neuroscience Methods, 206(2), 120-131. doi:https://doi.org/10.1016/j.jneumeth.2012.02.013

Steenken, F., Oetjen, H., Beutelmann, R., Carney, L. H., Koeppl, C., & Klump, G. M. (2022). Neural processing and perception of Schroeder-phase harmonic tone complexes in the gerbil: Relating single-unit neurophysiology to behavior. European Journal of Neuroscience, 56(3), 4060-4085. doi:https://doi.org/10.1111/ejn.15744

Suga, N. (1965). Analysis of frequency-modulated sounds by auditory neurones of echo-locating bats. J Physiol, 179(1), 26-53. doi:10.1113/jphysiol.1965.sp007648

Woolley, S. M. N., Gill, P. R., Fremouw, T., & Theunissen, F. E. (2009). Functional Groups in the Avian Auditory System. The Journal of Neuroscience, 29(9), 2780-2793. doi:10.1523/jneurosci.2042-08.2009

Yin, T. C. T., Smith, P. H., & Joris, P. X. (2019). Neural Mechanisms of Binaural Processing in the Auditory Brainstem. Compr Physiol, 9(4), 1503-1575. doi:10.1002/cphy.c180036